Molecular Cell, Volume *49*

Supplemental Information

Dissection of DNA Damage Responses

Using Multiconditional Genetic Interaction Maps

Aude Guénolé, Rohith Srivas, Kees Vreeken, Ze Zhong Wang, Shuyi Wang, Nevan J. Krogan, Trey Ideker, and Haico van Attikum

Supplemental Experimental Procedures

Assessing the Quality of the Genetic Interaction Data

To ensure a high-quality dataset we examined several different quality control metrics:

(i) Correlation of replicate colony size measurements: Each query mutant in this screen was crossed against all array mutants six different times for each condition (Untreated, MMS, ZEO, and CPT). Figure S1A displays the histogram of the average correlation seen amongst the colony size measurements made across the six replicates for each query in each condition. The average Pearson's correlation seen amongst replicates was 0.78.

(ii) Correlation of NAT x KAN swaps: A subset of interactions in this dataset were screened twice with the only difference being the orientation of the drug resistance markers, i.e., *xxx*Δ::KAN *yyy*Δ::NAT versus *xxx*Δ::NAT *yyy*Δ::KAN. Each of these 'swaps' were scored independently. Across all four conditions, we observed a high correlation between the genetic interactions scores (S score) for these 'swap' replicates (Figures S1B-E). These correlation values are in line with previously published datasets (Collins et al., 2006; Roguev et al., 2008).

(iii) Examination of linkage plots: Although each query mutant was checked via colony PCR for insertion of the drug resistance marker at the proper genomic location, it is not uncommon for ~10-15% of strains screened to be incorrect (Collins et al., 2010; Collins et al., 2006). One useful tool for identifying these incorrect strains is to examine the interaction scores for pairs of genes that are located relatively close to one another in the genome. Due to linkage, such strains will fail to inherit both drug resistance markers following sporulation and as a result will appear as a negative interaction when plated on double selection media. As Figure S1F shows gene-pairs located within 100 kbp of each other tended to exhibit a much more negative S score, indicating that the majority of strains are indeed correct. Individual strains which deviated from this trend were identified and removed from the final dataset.

(iv) Agreement with previously published low-throughput genetic interaction data: We downloaded all reported low-throughput genetic interactions from the BioGRID database (Stark et al., 2006) on May 7th, 2012 and examined how well our untreated static network could recover these interactions. As shown in Figure S1G, we see a high enrichment (> 5 fold) for these 'gold-standard' interactions amongst the top 5% of our interactions, indicating good agreement.

(v) Agreement with previously published high-throughput genetic interaction data: We examined how well the genetic interaction scores in our untreated network aligned with

genetic interaction data generated in five previously published E-MAP screens (Collins et al., 2007b; Fiedler et al., 2009; Hoppins et al., 2011; Wilmes et al., 2008; Zheng et al., 2010). Our scores were highly correlated with this previously published data ($r \geq 0.5$) and performed as well as the untreated network from our previously published dE-MAP (Bandyopadhyay et al., 2010) (Figure S1H).

Next, we considered the possibility that our particular experimental design (i.e., a relatively small number of functionally related queries) may affect the quality of either the static or differential genetic interaction scores. However, we feel that this is unlikely to be a large issue for several reasons. First, a recent review paper analyzed what effect the number of query genes in a screen had on the quality of the data (Collins et al., 2010). The authors concluded that screens with <20 query genes may have substantial error, while each additional query beyond 40 query genes provides only marginal improvement. With these considerations in mind we designed a screen involving 55 query genes, ensuring that our dataset would not be subject to this particular source of error.

Another potential issue is since our set of queries are somewhat functionally related, the situation may arise in which a given array gene would interact with a high percentage of all query genes. Since the E-MAP scoring methodology estimates the expected double mutant colony size for each array gene separately by using the peak of the distribution of all double mutant (containing the array gene in question) colony sizes, an array gene which interacts strongly with many queries would skew this distribution and hence the estimate of the expected double mutant colony size (Collins et al., 2006). However, the E-MAP scoring procedure features a number of computational procedures designed to explicitly account for this situation (Collins et al., 2006). Rather than use either the mean or median of the distribution double mutant colony sizes as the expected double mutant colony size, a kernel density estimation (Duda and Hart, 1973) is fit to the distribution and the peak value of this fitted distribution is subsequently used. In this way the estimate of the expected double mutant colony size is less sensitive to outliers (Collins et al., 2010; Collins et al., 2006). In addition, rather than using the actual variance of this distribution for each individual array gene in computing the S score, a pooled variance measure is used instead, which leverages information across all of the array genes in the screen. Again, this procedure helps to negate the effect of outliers in estimating the expected double mutant colony size and has been shown to significantly improve the reproducibility of genetic interactions (Baryshnikova et al., 2010; Collins et al., 2006).

Finally, the methodology we use to identify significant differential genetic interactions does not incorporate, either explicitly or implicitly, the dimensions or functional representation of the interaction screen. In brief, for each gene pair we compute the difference in S scores between treated and untreated conditions and assess the significance of this difference in reference to a null distribution of differences derived from replicate genetic interaction screens from the same condition (Bandyopadhyay et al., 2010). Moreover, as the various quality control metrics we have examined attest to the high quality and reproducibility of the static S scores (Figure S1), we do not feel that the experimental design affects the differential p-values calculated here.

Assessing the False Discovery Rate (FDR) of Differential Genetic Interactions

To assess the false discovery rate (FDR) of the differential genetic interactions, we corrected the differential p-value assigned to each gene-pair across all three conditions using the Benjamini-

Hochberg procedure. At $P \leq 0.002$, the threshold used in this study, we observed an FDR of 6.2%, 17.4%, and 13.2% respectively for the MMS, CPT, and ZEO differential networks (Figure S1I).

Functional enrichment analysis

Both static and differential genetic networks were examined for enrichment of interactions with various sets of functionally related genes (Table S3). Significance was assessed using the hypergeometric distribution where the four parameters were defined as follows:

k. Total number of significant interactions containing a gene involved in a function of interest (e.g. DNA repair).

m. Total number of tested interactions containing a gene involved in a function of interest.

n. Total number of significant genetic interactions.

N. Total number of tested genetic interactions.

A significant differential genetic interaction was defined as having a differential p-value below 0.002. A significant static genetic interaction was defined as $S \geq 2.0$ or $S \leq -2.5$. The total number of tested interactions was the same across both static and differential networks (97,578). The enrichment results presented in Figure 2A were robust to the choice of significance threshold (Figures S2A–B) as well as alternate definitions of DNA repair genes or chromatin organization genes (Figure S2C).

Clustering Analysis of Static and Differential Genetic Interactions

To generate Supplemental Figures S2B–C, we hierarchically clustered the 220 (55 query genes x 4 conditions) by 2022 (# of array genes) matrix containing static interaction scores as well as the 165 (55 query genes x 3 pair-wise comparisons) by 2022 matrix containing differential interaction scores. Here, the differential interaction score is defined as:

Differential Score = $\text{sign}(S_{treated}-S_{untreated}) \times -\log_{10}(p_{diff})$

where,

$S_{treated}$ = S score (static interaction score) in a treated condition

$S_{untreated}$ = S score in untreated condition

P_{diff} = the differential p-value assigned to each interaction, which represents both the magnitude and confidence in the change in genetic interaction between treated and untreated conditions.

The matrices were clustered using the hclust function in R (version 2.14.0) with default parameters (Euclidean distance, complete linkage), after which the leaves were re-ordered using the order.optimal function in the R package cba (Bar-Joseph et al., 2001). The resulting dendrogram was visualized using the ColorDendrogram function in the R package sparcl (version 1.0.2) (Witten and Tibshirani, 2010).

Description of Single Mutant and Gene Expression Datasets Used In This Study

We obtained single mutant data from a previously published chemogenetic screen which had examined the fitness of 4,722 homozygous diploid mutants in response to hundreds of different compounds (Hillenmeyer et al., 2008). To ensure the closest comparison with the perturbations in this study, we used fitness data generated under the following concentrations: MMS (0.002%) and CPT (30 μg/mL). For ZEO, we used the fitness data generated under bleomycin (1.7 μg/mL), a chemical compound which induces similar effects to zeocin. Differential gene expression data for MMS (0.12%) and ZEO (again using data generated under bleoymycin [0.15

U/ml]) were obtained from Caba and colleagues (Caba et al., 2005). Expression data for CPT were obtained from Travesa and colleagues (Travesa et al., 2012).

Testing for Association Between Agent and DNA Repair Pathway

For each experimental technology, we generated a 3x6 contingency table (C), where each cell ($C_{i,j}$) was defined as follows:

Differential networks: $C_{i,j}$ is the number of significant differential interactions observed in condition *i* containing a gene in pathway *j*.

Single mutant data: $C_{i,j}$ is the number of genes displaying a significant sensitivity in condition *i* which also fall in pathway *j*.

Gene expression data: $C_{i,j}$ is the number of differentially expressed genes observed in condition *i* which are also in pathway *j* where i ∈ {MMS, CPT, ZEO} and j ∈ {Double-strand break repair, DNA damage checkpoint, nucleotide excision repair, mismatch repair, post-replication repair, base excision repair}. All pathway definitions have been provided in Table S3.

A standard chi-square statistic (X^2) was then computed on this contingency table. To assess significance, the chi-square statistic was re-calculated over 1000 permutations in which the set of sensitive genes or differentially expressed genes were randomly re-assigned to a different compound, while ensuring (i) the total number sensitive/differentially expressed genes seen in the actual data was maintained in each permutation and, (ii) any dependencies seen amongst compounds was maintained in the permutation, i.e., if there were 40 differentially expressed genes seen in both MMS and CPT, the same number was maintained in each permutation. For the differential networks, we generated 1000 randomized networks by scrambling the node labels, after which the chi-square statistic was re-computed. This null distribution of chi-square statistics was subsequently used to assign each experimental technology a p-value for the association between agent and pathway.

Constructing a map of DNA Damage Response Processes

A list of biological processes was downloaded from the Gene Ontology (GO) database (Ashburner et al., 2000) on July 5th, 2012. This list was filtered to include only those terms which were below the ninth level of the GO hierarchy, contained at least two query or array genes, and had less than 100 genes annotated to it. The final list contained 632 biological processes (Table S6). Each process and pair of processes was then examined for an enrichment of differential genetic interactions as previously described (Hannum et al., 2009).

We found that differential interactions were far more likely to span pairs of processes rather than enrich within individual processes. In total, we identified 687 pairs of functional processes spanned by a significant number of differential interactions ($P' < 0.05$; P' is a Bonferroni-corrected p-value) indicating extensive differential genetic crosstalk. On the other hand, our analysis found only 10 functional processes that were enriched for differential interactions ($P' < 0.05$); in contrast, 49 distinct processes were enriched for static interactions. These results suggest that the crosstalk between discrete functional processes, rather than within these processes, is re-wired in response to these DNA damaging agents. This finding mirrors what we and others (Bandyopadhyay et al., 2010) have observed at the level of protein complexes. This map of functional processes has been provided as a Cytoscape session file

(Supplementary Data Set S1; available on our Supplementary Website – http://chianti.ucsd.edu/~rsrivas/guenole_2012/index.html) and can be viewed/searched using Cytoscape (version 2.8.2 or above), which is available as a free download from http://cytoscape.org/.

Integrative analysis of differential genetic interactions and protein interactions

Protein interactions were obtained from a previous integration of several primary protein interaction screens (Collins et al., 2007a), from which we selected interactions with PE >= 2.0. Each static network was analyzed using a previously published workflow to identify multi-genic modules, i.e. sets of genes spanned by many physical and genetic interactions (Srivas et al., 2011), using the following parameters: module size reward = -1.6, network filter degree = 2, edge reporting = 0.1. This list was further augmented with a set of literature-curated protein complexes (Pu et al., 2009), resulting in a final set of 332 modules after removing overlapping modules (Table S4). To identify functional relationships between modules, we searched for enrichment of significant differential genetic interactions (both positive and negative) between each module pair. Significance was assessed using the hypergeometric distribution as previously described (Hannum et al., 2009). We then applied a threshold of $P \leq 0.05$ to arrive at a final network consisting of 179 modules (color coded green in Table S4) and 452 inter-module links (Table S5).

To place our differential genetic interaction data within the context of the existing untreated static genetic interaction data available in *S. cerevisiae*, we obtained a nearly genome-wide genetic interaction dataset from a recent publication (Ryan et al., 2012), which had integrated genetic interaction data from over nine different screens (Aguilar et al., 2010; Bandyopadhyay et al., 2010; Collins et al., 2007b; Costanzo et al., 2010; Fiedler et al., 2009; Hoppins et al., 2011; Schuldiner et al., 2005; Wilmes et al., 2008; Zheng et al., 2010). This merged dataset comprised over 4.7 million genetic interactions amongst 4,438 genes (~89% of all verified yeast genes). We analyzed this network as described above (using identical parameters) to identify multi-genic modules. This list of modules were subsequently merged with our previous set of modules (Table S4), after which we assessed each module pair for an enrichment of differential genetic interactions (in each of three conditions), as well as static genetic interactions. This resulted in a module map of 277 modules and 1895 inter-module links (again using a threshold of $P \leq 0.05$). To enable readers to easily search and visualize the map, we have packaged it as a Cytoscape session file (Supplementary Data Set S2; available on our Supplementary Website – http://chianti.ucsd.edu/~rsrivas/guenole_2012/index.html). Unlike our previous module map (Figure 5A), this map contains inter-module links comprised of both untreated static genetic interactions (black edges) and differential genetic interactions (red edges). The inter-module links identified by the static and differential genetic networks were largely separate with only 33 common interactions (green edges), demonstrating the complementary nature of the two networks.

To further enhance the utility of this expanded module map, we integrated it with data obtained from a number of high-throughput screens including: (i) assignment of 799 genes to phases of the cell cycle (G1, G2, G2/M, S) based on their peak phase of expression (Spellman et al., 1998), (ii) single mutant sensitivity measurements for 4,722 genes in response to MMS, CPT, and ZEO (Hillenmeyer et al., 2008), (iii) over-expression growth rate measurements for 769 genes (Sopko et al., 2006), and (iv) Effect of gene deletions on the levels of spontaneous Rad52 foci formation (a metric of DNA repair activity) (Alvaro et al., 2007). For each of these

orthogonal datasets we have generated custom visualization styles. For example, applying the Rad52 Foci Overlay style, colors the modules according to the extent to which the module affects the assembly of Rad52 foci. Applying the Cell Cycle Phase Expression Overlay style, colors the modules according to the specific phase of the cell cycle in which peak expression is seen for its constitutive genes. Applying the Overexpression Phenotype Overlay style, colors modules according to their sensitivity seen due to over-expression of their constitutive genes. Applying the CPT Sensitivity Overlay, MMS Sensitivity Overlay, or ZEO Sensitivity Overlay visual style, colors modules according to their sensitivity to the respective DNA damaging agent.

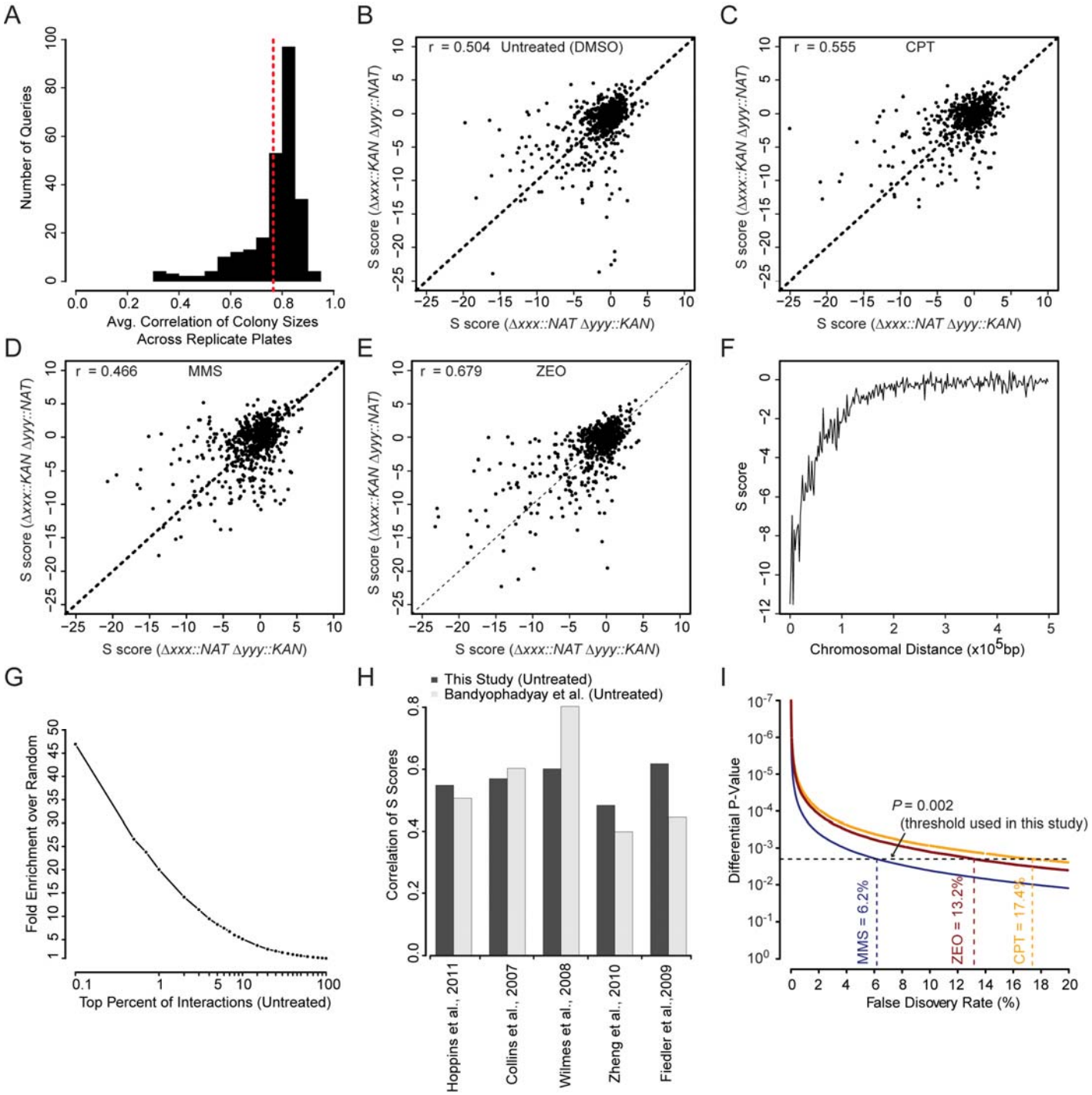

Figure S1. Quality of genetic interaction data, Related to Figure 1

(A) Each query mutant was crossed against the set of array mutants six different times. This histogram displays the average correlation seen in colony size measurements between the six replicates for each query across all four conditions (Untreated, MMS, CPT, and ZEO). The dotted red-line indicates the average correlation seen across all queries and all conditions (r = 0.78). (B–E) Correlation of genetic interaction scores derived from 'marker swap' experiments for (B) Untreated, (C) CPT, (D) MMS, and (E) ZEO. (F) Genetic interaction scores for pairs of genes in linkage. (G) The fold-enrichment for low-throughput genetic interactions from the

Biogrid database (Stark et al., 2006) is shown. Fold-enrichment is defined as n/r, where n is the number of highest scoring static genetic interactions in untreated conditions (x-axis) found in the Biogrid database, while r is the number of overlapping interactions expected at random. (H) Correlation of S scores measured under untreated conditions from this study (dark grey) or a previously published dE-MAP (Bandyopadhyay et al., 2010) (light grey) versus five large genetic interaction screens. (I) The differential p-value (x-axis) is plotted versus the corresponding multiple hypothesis corrected false discovery rate (FDR) (corrected using the Benjamini-Hochberg procedure) for each condition.

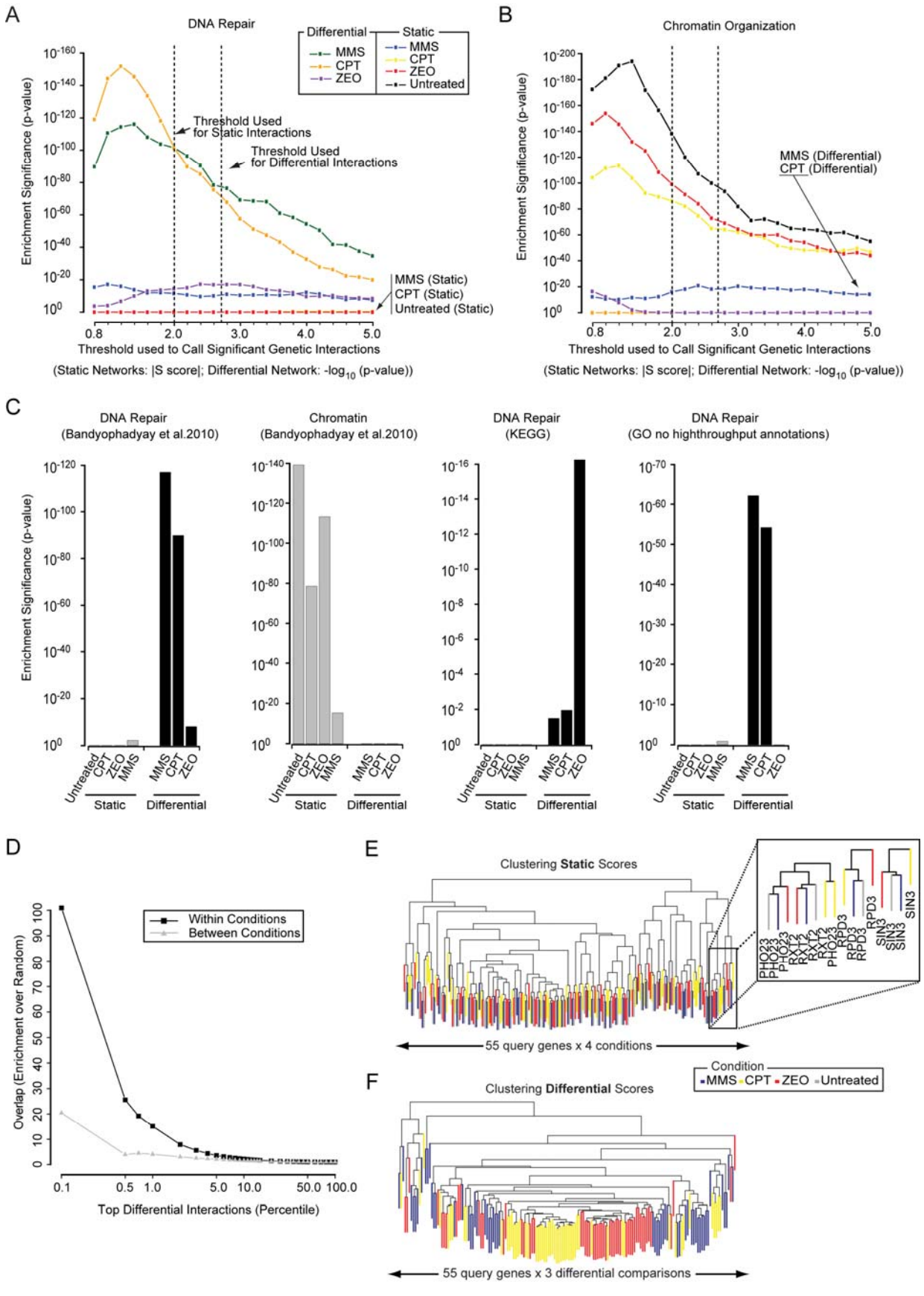
A
DNA Repair
Differential
Static
MMS
CPT
ZEO
Untreated
Threshold Used for Static Interactions
Threshold Used for Differential Interactions
MMS (Static)
CPT (Static)
Untreated (Static)
Enrichment Significance (p-value)
Threshold used to Call Significant Genetic Interactions
(Static Networks: |S score|; Differential Network: -log10 (p-value))
B
Chromatin Organization
MMS (Differential)
CPT (Differential)
C
DNA Repair (Bandyophadyay et al.2010)
Chromatin (Bandyophadyay et al.2010)
DNA Repair (KEGG)
DNA Repair (GO no highthroughput annotations)
Static
Differential
D
Within Conditions
Between Conditions
Overlap (Enrichment over Random)
Top Differential Interactions (Percentile)
E
Clustering Static Scores
55 query genes x 4 conditions
Condition
F
Clustering Differential Scores
55 query genes x 3 differential comparisons

Figure S2. Comparison of replicate differential genetic networks and robustness of functional enrichment results, Related to Figure 2

(A-B) The significance of enrichment for interactions with either (A) DNA repair or (B) chromatin organization genes is plotted for all static and differential genetic networks across a range of thresholds. For static networks the absolute value of the S score is used as a threshold. For differential networks the $-\log_{10}$ (differential p-value) is used as a threshold. (C) Enrichment results using different databases to define gold-standard genes involved in DNA repair and chromatin organization. (D) The overlap in replicate differential networks seen amongst the same condition (black line) or between two different conditions (grey line). Replicate networks were derived by splitting the six replicates obtained for each double mutant into two sets and by scoring each set independently. Enrichment over random (y-axis) is defined as the ratio of overlapping interactions seen between replicate networks amongst the top percent of differential interactions (x-axis) to the number of overlapping interactions expected at random. (E) Dendrogram of each query gene in each of four conditions (Untreated, MMS, CPT, and ZEO) generated by hierarchically clustering their static genetic interaction patterns across 2022 array genes. The leaves of the dendrogram have been colored according to the condition. The insert shows an expanded view of one branch of the dendrogram. (F) As in E, except that the dendrogram is generated by hierarchically clustering the differential interaction profiles for each query gene in each of three pairwise differential comparisons (MMS vs. Untreated, CPT vs. Untreated, ZEO vs. untreated). Leaves of the dendrogram have been colored as in E.

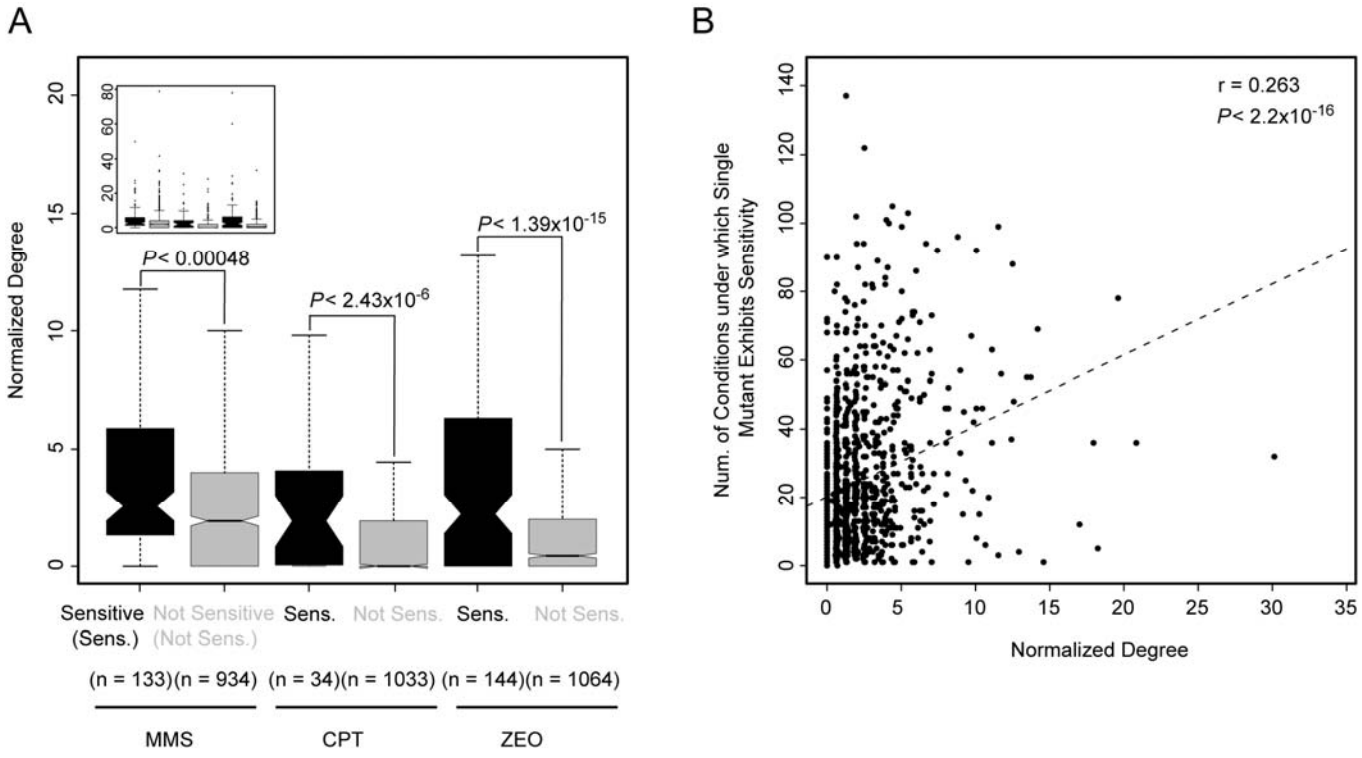

Figure S3. Differential genetic hubs display greater DNA damage sensitivity and tend to display pleiotropy, Related to Figure 3

(A) All genes considered in this screen are binned according to their single mutant sensitivity to MMS, CPT, or ZEO. The distribution of the normalized differential degree (# sig. interactions / # tested interactions) for the genes in each bin is summarized with a box-and-whisker plot. The inset shows the full range of the distribution of normalized degrees, while the main plot shows a zoomed-in portion. A p-value was calculated using the Mann-Whitney test. (B) The Hillenmeyer et al. study (Hillenmeyer et al., 2008) measured single-gene knockout sensitivities to over 400 different compounds. The normalized degree for each gene considered in this study is plotted against the number of drugs for which the gene knockout is sensitive.

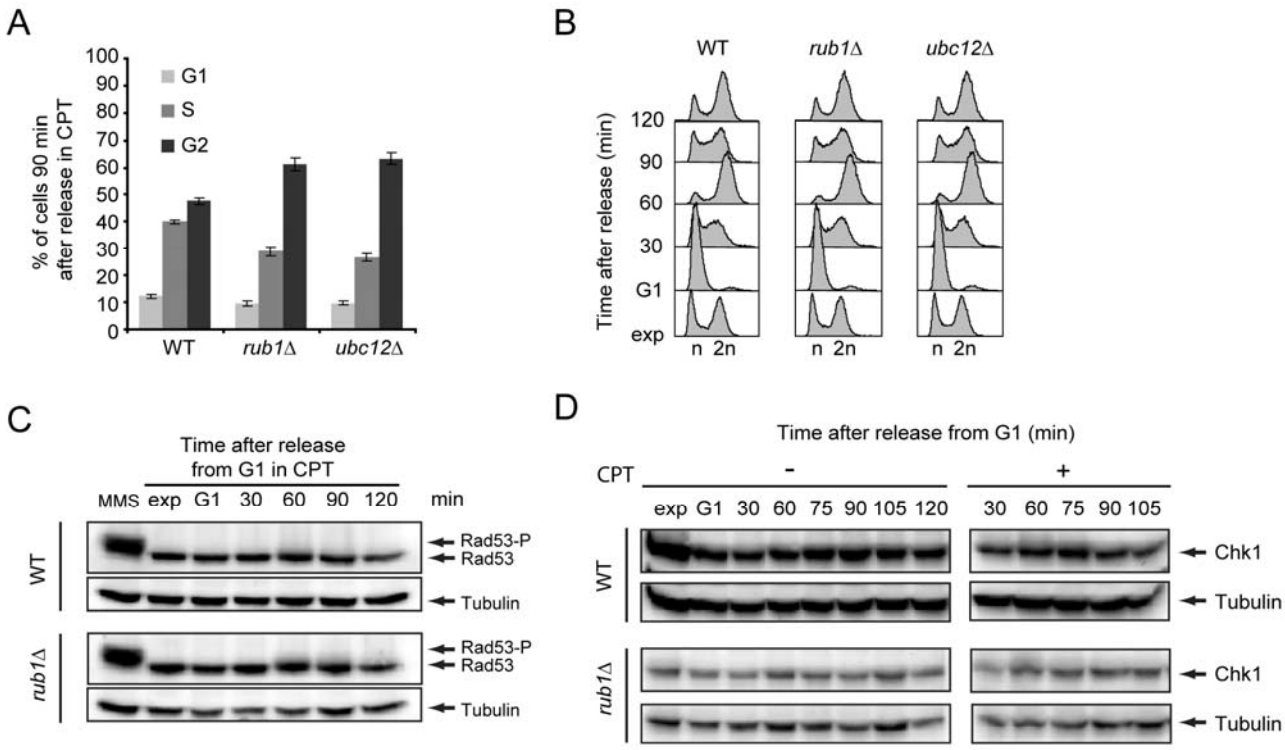

Figure S4. Neddylation regulates cell cycle progression after DNA damage, Related to Figure 4

(A) Quantification of FACS data from Figure 4E. The bar-plot represents the percentage of wild-type (WT), *rub1*Δ and *ubc12*Δ cells in G1, S or G2 phase 90 minutes after their release from G1 in fresh medium containing CPT. Data represent the mean ± standard deviation from three independent experiments. (B) Exponentially (exp) growing WT, *rub1*Δ and *ubc12*Δ cells were arrested in G1 with α-factor and released in fresh medium. Cells were analyzed by FACS at the indicated time points. (C-D) Exponentially (exp) growing WT and *rub1*Δ cells were arrested in G1 with α-factor and released in fresh medium containing CPT (50 μM). MMS-treated exponentially growing cells served as a positive control. The phosphorylation status of (C) Rad53 and (D) Chk1 was monitored using Western blot analysis at the indicated time-points.

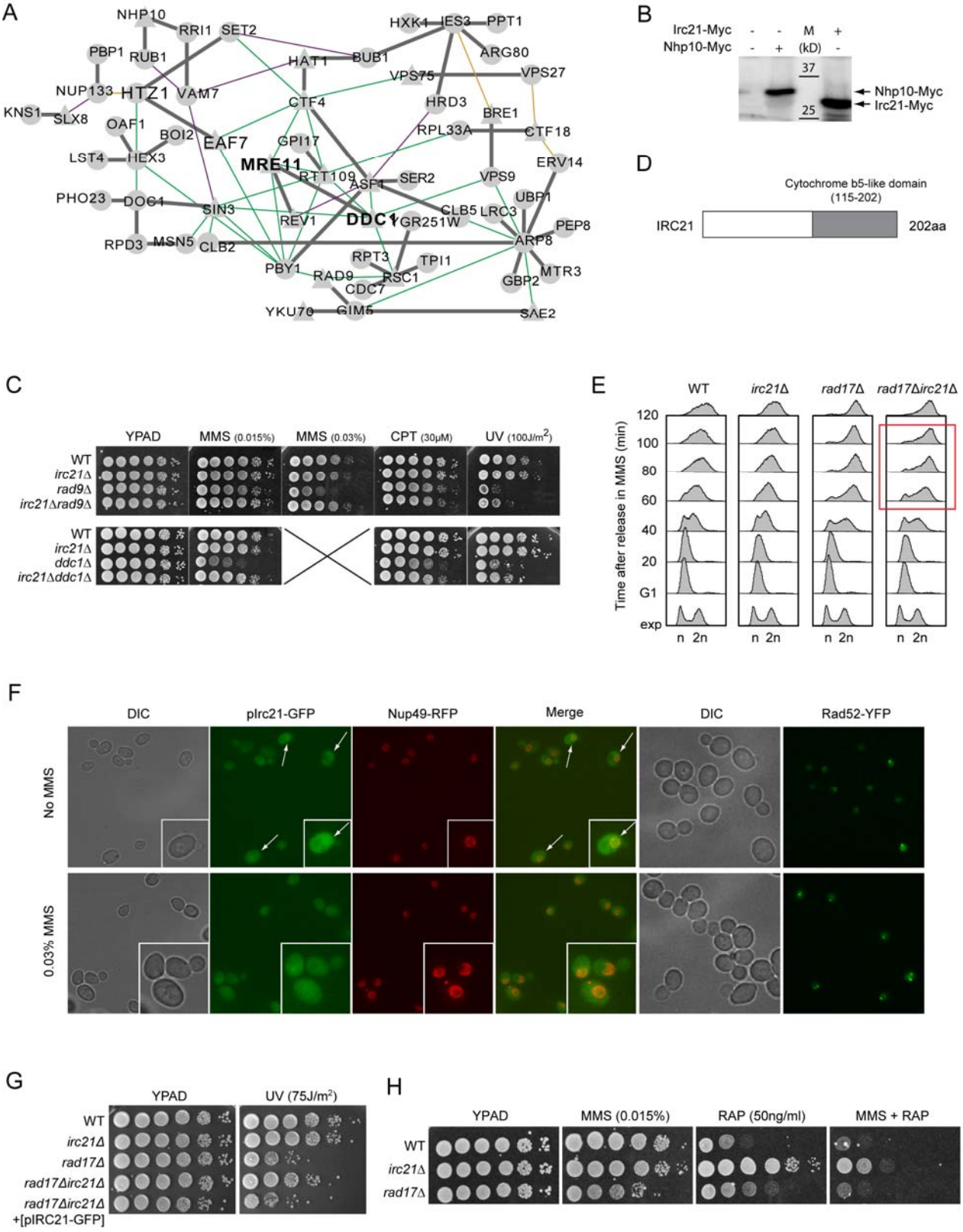
A
NHP10
RRI1
SET2
HXK1
IES3
PPT1
PBP1
RUB1
HAT1
BUB1
ARG80
VPS75
VPS27
NUP133
HTZ1
VAM7
CTF4
HRD3
KNS1
SLX8
OAF1
BRE1
RPL33A
CTF18
BOI2
EAF7
GPI17
LST4
HEX3
MRE11
ERV14
RTT109
ASF1
SER2
VPS9
PHO23
DOC1
UBP1
SIN3
REV1
DDC1
CLB5
LRC3
YGR251W
PEP8
RPD3
MSN5
CLB2
ARP8
RPT3
TPI1
PBY1
RAD9
RSC1
MTR3
CDC7
GBP2
YKU70
GIM5
SAE2
B
Irc21-Myc
Nhp10-Myc
M
(kD)
37
25
Nhp10-Myc
Irc21-Myc
D
Cytochrome b5-like domain
(115-202)
IRC21
202aa
C
YPAD
MMS (0.015%)
MMS (0.03%)
CPT (30μM)
UV (100J/m2)
WT
irc21Δ
rad9Δ
irc21Δrad9Δ
WT
irc21Δ
ddc1Δ
irc21Δddc1Δ
E
WT
irc21Δ
rad17Δ
rad17Δirc21Δ
Time after release in MMS (min)
120
100
80
60
40
20
G1
exp
n 2n
F
DIC
pIrc21-GFP
Nup49-RFP
Merge
DIC
Rad52-YFP
No MMS
0.03% MMS
G
YPAD
UV (75J/m2)
WT
irc21Δ
rad17Δ
rad17Δirc21Δ
rad17Δirc21Δ
+[pIRC21-GFP]
H
YPAD
MMS (0.015%)
RAP (50ng/ml)
MMS + RAP
WT
irc21Δ
rad17Δ

Figure S5. Irc21 localizes in both the cytoplasm and nucleus, shows differential genetic interactions with components of DNA damage checkpoints and may be linked to mTOR signaling, Related to Figure 5

(A) Network of differential genetic interactions conserved in all three conditions (dark grey edges) or in two of three conditions (green edges = CPT & MMS; orange edges = CPT & ZEO; purple edges = ZEO & MMS). Triangular nodes represent genes known to be involved in DNA repair. (B) Western blot analysis of cells expressing Myc-tagged Irc21. Cells from non-tagged and Nhp10-Myc expressing strains were used as negative and positive controls, respectively. (C) *IRC21* deletion rescues the viability of *rad9*Δ and *ddc1*Δ cells in the presence of DNA damaging agents. 10-fold serial dilutions of log-phase cells of the indicated genotypes were either spotted onto YPAD plates containing MMS or CPT, or spotted on YPAD and exposed to UV, and incubated for 3 days at 30°C. (D) Schematic of the Irc21 protein showing a cytochrome b5-like domain in its C-terminus. **(**E**)** Exponentially (exp) growing wild-type (WT), *irc21*Δ, *rad17*Δ, *rad17*Δ*irc21*Δ cells were arrested in G1 with α-factor and released in fresh medium containing 0.02% MMS and 15μg nocodazole. Cells were analyzed by FACS at the indicated time points**.** (F) Exponentially growing *irc21*Δ cells expressing Irc21-GFP and Nup49-RFP were treated with 0.03% MMS for 1 hour and then examined for Irc21 localization. Wild-type cells expressing Rad52-YPF were treated similarly and examined for Rad52 focus formation. (G) Ectopic expression of Irc21-GFP in *rad17*Δ*irc21*Δ renders cells as sensitive to UV as *rad17*Δ cells, demonstrating the functionality of GFP-tagged Irc21. 10-fold serial dilutions of log-phase cells of the indicated genotypes were spotted onto YPAD plates, exposed to UV and incubated for 3 days at 30°C. (H) *irc21*Δ cells are hypersensitive to MMS when combined with the TOR inhibitor rapamycin (RAP). 10-fold serial dilutions of log-phase cells of the indicated genotypes were either spotted onto YPAD plates containing MMS, RAP or both and incubated for 3 days at 30°C.

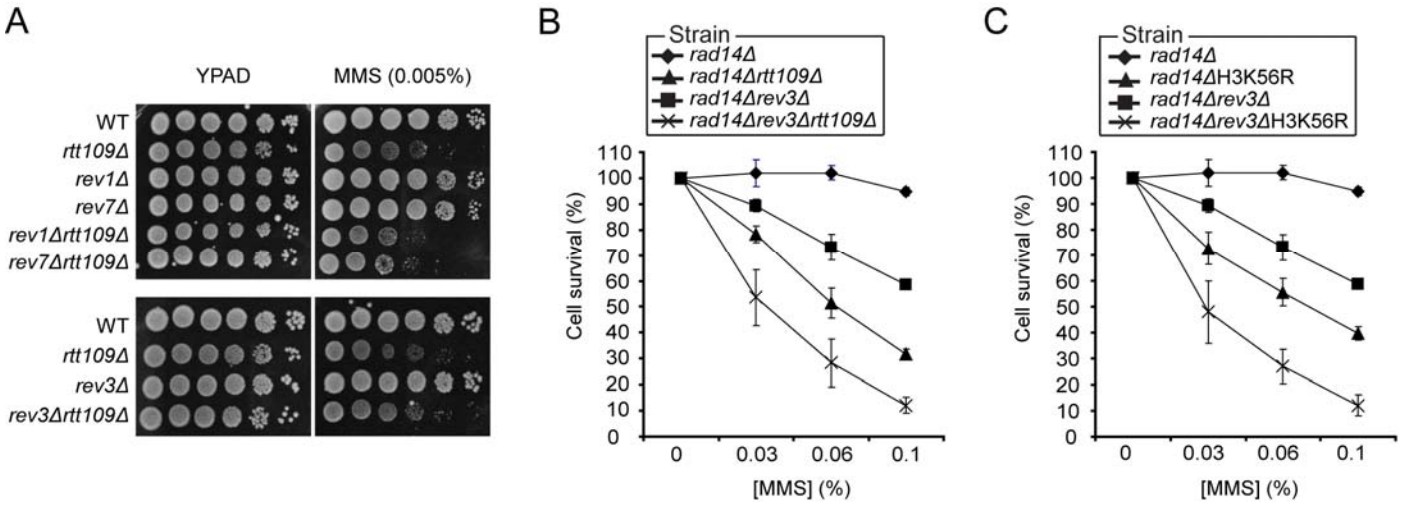

Figure S6. Integrative analysis of differential genetic interactions reveals a role for RTT109 in translesion synthesis, Related to Figure 6

(A) *RTT109* displays epistatic interactions with components of the polymerase ζ complex (*REV1*, *REV3*, *REV7*) in the presence MMS. 10-fold serial dilutions of log-phase cells of the indicated genotypes were spotted onto YPAD plates containing MMS and incubated for 3 days at 30°C. (B) MMS survival of NER-deficient *rad14*Δ, *rad14*Δ*rev3*Δ, *rad14*Δ*rtt109*Δ and *rad14*Δ*rev3*Δ*rtt109*Δ, and of (C) NER-deficient *rad14*ΔH3K56R and *rad14*Δ*rev3*ΔH3K56R cells were examined. Log-phase cells were exposed for 20 minutes to the indicated MMS concentrations. Appropriate dilutions of were plated on SC(-Arg) and colony formation was scored. The data represent the mean ± 1 s.d. of three independent experiments.

Data Set S1. Related to Figure 6
A Cytoscape session file which contains a map of DNA damage processes and the differential genetic crosstalk between these processes (available on our Supplementary Website - http://chianti.ucsd.edu/~rsrivas/guenole_2012/index.html). This file can be opened using Cytoscape version 2.8.2 or above. Cytoscape can be obtained as a free download from http://cytoscape.org/.

Data Set S2. Related to Figure 6
A Cytoscape session file which contains a module map constructed from previously published genetic interaction data in *S. cerevisiae* (available on our Supplementary Website - http://chianti.ucsd.edu/~rsrivas/guenole_2012/index.html). This file can be opened using Cytoscape version 2.8.2 or above.

Supplemental References

Aguilar, P.S., Frohlich, F., Rehman, M., Shales, M., Ulitsky, I., Olivera-Couto, A., Braberg, H., Shamir, R., Walter, P., Mann, M.*, et al.* (2010). A plasma-membrane E-MAP reveals links of the eisosome with sphingolipid metabolism and endosomal trafficking. Nature structural & molecular biology *17*, 901-908.

Alvaro, D., Lisby, M., and Rothstein, R. (2007). Genome-wide analysis of Rad52 foci reveals diverse mechanisms impacting recombination. PLoS genetics *3*, e228.

Ashburner, M., Ball, C.A., Blake, J.A., Botstein, D., Butler, H., Cherry, J.M., Davis, A.P., Dolinski, K., Dwight, S.S., Eppig, J.T.*, et al.* (2000). Gene ontology: tool for the unification of biology. The Gene Ontology Consortium. Nature genetics *25*, 25-29.

Bandyopadhyay, S., Mehta, M., Kuo, D., Sung, M.K., Chuang, R., Jaehnig, E.J., Bodenmiller, B., Licon, K., Copeland, W., Shales, M.*, et al.* (2010). Rewiring of genetic networks in response to DNA damage. Science *330*, 1385-1389.

Bar-Joseph, Z., Gifford, D.K., and Jaakkola, T.S. (2001). Fast optimal leaf ordering for hierarchical clustering. Bioinformatics *17 Suppl 1*, S22-29.

Baryshnikova, A., Costanzo, M., Kim, Y., Ding, H., Koh, J., Toufighi, K., Youn, J.Y., Ou, J., San Luis, B.J., Bandyopadhyay, S.*, et al.* (2010). Quantitative analysis of fitness and genetic interactions in yeast on a genome scale. Nature methods *7*, 1017-1024.

Caba, E., Dickinson, D.A., Warnes, G.R., and Aubrecht, J. (2005). Differentiating mechanisms of toxicity using global gene expression analysis in Saccharomyces cerevisiae. Mutation research *575*, 34-46.

Collins, S.R., Kemmeren, P., Zhao, X.C., Greenblatt, J.F., Spencer, F., Holstege, F.C., Weissman, J.S., and Krogan, N.J. (2007a). Toward a comprehensive atlas of the physical interactome of Saccharomyces cerevisiae. Molecular & cellular proteomics : MCP *6*, 439-450.

Collins, S.R., Miller, K.M., Maas, N.L., Roguev, A., Fillingham, J., Chu, C.S., Schuldiner, M., Gebbia, M., Recht, J., Shales, M.*, et al.* (2007b). Functional dissection of protein complexes involved in yeast chromosome biology using a genetic interaction map. Nature *446*, 806-810.

Collins, S.R., Roguev, A., and Krogan, N.J. (2010). Quantitative genetic interaction mapping using the E-MAP approach. Methods in enzymology *470*, 205-231.

Collins, S.R., Schuldiner, M., Krogan, N.J., and Weissman, J.S. (2006). A strategy for extracting and analyzing large-scale quantitative epistatic interaction data. Genome biology *7*, R63.

Costanzo, M., Baryshnikova, A., Bellay, J., Kim, Y., Spear, E.D., Sevier, C.S., Ding, H., Koh, J.L., Toufighi, K., Mostafavi, S.*, et al.* (2010). The genetic landscape of a cell. Science *327*, 425-431.

Duda, R.O., and Hart, P.E. (1973). Pattern classification and scene analysis (New York,, Wiley).

Fiedler, D., Braberg, H., Mehta, M., Chechik, G., Cagney, G., Mukherjee, P., Silva, A.C., Shales, M., Collins, S.R., van Wageningen, S.*, et al.* (2009). Functional organization of the S. cerevisiae phosphorylation network. Cell *136*, 952-963.

Hannum, G., Srivas, R., Guenole, A., van Attikum, H., Krogan, N.J., Karp, R.M., and Ideker, T. (2009). Genome-wide association data reveal a global map of genetic interactions among protein complexes. PLoS genetics *5*, e1000782.

Hillenmeyer, M.E., Fung, E., Wildenhain, J., Pierce, S.E., Hoon, S., Lee, W., Proctor, M., St Onge, R.P., Tyers, M., Koller, D.*, et al.* (2008). The chemical genomic portrait of yeast: uncovering a phenotype for all genes. Science *320*, 362-365.

Hoppins, S., Collins, S.R., Cassidy-Stone, A., Hummel, E., Devay, R.M., Lackner, L.L., Westermann, B., Schuldiner, M., Weissman, J.S., and Nunnari, J. (2011). A mitochondrial-focused genetic interaction map reveals a scaffold-like complex required for inner membrane organization in mitochondria. The Journal of cell biology *195*, 323-340.

Pu, S., Wong, J., Turner, B., Cho, E., and Wodak, S.J. (2009). Up-to-date catalogues of yeast protein complexes. Nucleic acids research *37*, 825-831.

Roguev, A., Bandyopadhyay, S., Zofall, M., Zhang, K., Fischer, T., Collins, S.R., Qu, H., Shales, M., Park, H.O., Hayles, J.*, et al.* (2008). Conservation and rewiring of functional modules revealed by an epistasis map in fission yeast. Science *322*, 405-410.

Ryan, C.J., Roguev, A., Patrick, K., Xu, J., Jahari, H., Tong, Z., Beltrao, P., Shales, M., Qu, H., Collins, S.R.*, et al.* (2012). Hierarchical Modularity and the Evolution of Genetic Interactomes across Species. Molecular cell *46*, 691-704.

Schuldiner, M., Collins, S.R., Thompson, N.J., Denic, V., Bhamidipati, A., Punna, T., Ihmels, J., Andrews, B., Boone, C., Greenblatt, J.F.*, et al.* (2005). Exploration of the function and organization of the yeast early secretory pathway through an epistatic miniarray profile. Cell *123*, 507-519.

Sopko, R., Huang, D., Preston, N., Chua, G., Papp, B., Kafadar, K., Snyder, M., Oliver, S.G., Cyert, M., Hughes, T.R.*, et al.* (2006). Mapping pathways and phenotypes by systematic gene overexpression. Molecular cell *21*, 319-330.

Spellman, P.T., Sherlock, G., Zhang, M.Q., Iyer, V.R., Anders, K., Eisen, M.B., Brown, P.O., Botstein, D., and Futcher, B. (1998). Comprehensive identification of cell cycle-regulated genes of the yeast Saccharomyces cerevisiae by microarray hybridization. Molecular biology of the cell *9*, 3273-3297.

Srivas, R., Hannum, G., Ruscheinski, J., Ono, K., Wang, P.L., Smoot, M., and Ideker, T. (2011). Assembling global maps of cellular function through integrative analysis of physical and genetic networks. Nature protocols *6*, 1308-1323.

Stark, C., Breitkreutz, B.J., Reguly, T., Boucher, L., Breitkreutz, A., and Tyers, M. (2006). BioGRID: a general repository for interaction datasets. Nucleic acids research *34*, D535-539.

Travesa, A., Kuo, D., de Bruin, R.A., Kalashnikova, T.I., Guaderrama, M., Thai, K., Aslanian, A., Smolka, M.B., Yates, J.R., 3rd, Ideker, T.*, et al.* (2012). DNA replication stress differentially regulates G1/S genes via Rad53-dependent inactivation of Nrm1. The EMBO journal.

Wilmes, G.M., Bergkessel, M., Bandyopadhyay, S., Shales, M., Braberg, H., Cagney, G., Collins, S.R., Whitworth, G.B., Kress, T.L., Weissman, J.S.*, et al.* (2008). A genetic interaction map of RNA-processing factors reveals links between Sem1/Dss1-containing complexes and mRNA export and splicing. Molecular cell *32*, 735-746.

Witten, D.M., and Tibshirani, R. (2010). A framework for feature selection in clustering. Journal of the American Statistical Association *105*, 713-726.

Zheng, J., Benschop, J.J., Shales, M., Kemmeren, P., Greenblatt, J., Cagney, G., Holstege, F., Li, H., and Krogan, N.J. (2010). Epistatic relationships reveal the functional organization of yeast transcription factors. Molecular systems biology *6*, 420.